Fermilab Library
0 1160 0047827 5

PRINT-95-170 (TSUKUBA)

Proposal to Observe the Long Range Component of the Nuclear Force in the Low Energy p-p Scattering

Tetsuo Sawada

Institute of Physics
University of Tsukuba
Ibaraki , 305 ,Japan

FERMILAB
AUG 23 1995
LIBRARY

Abstract

It is proposed to observe the effects of the long range component of the nuclear force by making precise measurements of the angular distribution of the cross section of the low energy p-p scatterings. Parameters of the long range force determined by the analysis of the once subtracted Kantor amplitude of the S-wave are used to predict the pattern of the destructive interference arising from the repulsive Coulomb force and the attractive long range force of the van der Waals type. It is shown that the most favorable energy range to carry out the experiments is $T_{lab} = 25 \sim 30 MeV.$, and the required accuracy of the measurement is higher than 0.08%, because the depth of the dip, which is characteristic to such an interference pattern, is -0.4%. Since the location of such a dip occurs at 12° of the scattering angle of the centre of mass system, measurements in the forward domain are necessary. Possible effects of the confirmation of the long range component of the nuclear force to the hadron physics are also discussed.

1. Introduction

Sixty years ago, Yukawa[1] proposed to understand the nuclear force in terms of the exchanges of a meson and a set of mesons with non-vanishing masses. Subsequent experimental discovery of the pion made his theory convincing. Today it is customary to regard the nuclear force as short range, and to retain only a few terms of the partial waves when we analyse the data of the low energy nucleon-nucleon scatterings.

On the other hand, in the most of the composite models of hadron, the constructive force among the constituent particles is the Coulombic type, and the long range force between hadrons emerges as a secondary force. To explain the situation of the appearance of the long range force, let us consider the dyon model of hadron due to Schwinger as a definite example. In such a magnetic monopole model of hadron[2], the constructive force is the super-strong magnetic Coulomb force acting between the constituent magnetic monopoles and the magnetically neutral composite system is identified with the hadron. This is analogous to the case of the ordinary atom, where the electric Coulomb force is the constructive force and the atom is the electrically neutral composite particle. Therefore in the magnetic monopole model of hadron, we can regard the hadrons as the "magnetic atoms". Since we know that the van der Waals force is acting between atoms, we can expect that the same mechanism gives rise to the van der Waals force betweem the magnetic atoms, namely between the hadrons.

Because of the charge quantization condition of Dirac, the electric charge e and the magnetic charge $^*e$ are quantized each other:[3]

$$\frac{^*ee}{\hbar c} = \frac{n}{2} \quad with \quad n = 0, \pm 1, \pm 2 \cdots \tag{1}$$

the smallness of the fine structure contant, namely $e^2/\hbar c = 1/137$, implies the largeness of the unit magnetic charge, that is $^*e^2/\hbar c = 137/4$. With such a super-strong funtamental Coulomb force, we can expect that the induced van der Waals force between hadrons still has the strength of the strong interaction[4]. Therefore there is no apriori reason to

believe that the nuclear force is strictly short range[5], rather it belongs to the problem to be determined only by experiments.

In this article, we analyse the low energy phase shift data of the proton-proton scattering in search for possible long range component of the nuclear force, and also propose to measure precisely the angular distribution of the cross section in $T_{lab} = 25 \sim 30 MeV$. region in search for the possible destructive interference pattern arising from the repulsive Coulomb force and the attractive long range force such as the strong van der Waals force. These two topics will be treated in Section 2 and Section 3, respectively.

In order to fix the notation, we shall write the spectral representation of the scattering amplitude $\tilde{A}(s,t)$, relation between the potential and the spectral function $\tilde{A}_t(s,t')$ and the explicite form of the cross section, which is to be measured by experiments of the proton-proton scatterings. We shall start by introducing two kinematical variables ν and θ, they are the momentum squared and the scattering angle in the center of the mass system. In the p-p interaction, the potential $V(r)$ is the sum of four terms:

$$V(r) = V_C(r) + V^{vac}(r) + V^{1\pi}(r) + \tilde{V}(r) \tag{2}$$

, where the first three terms of the r.h.s. are the Coulomb, vacuum polarization and the one-pion exchange potentials respectively, and their forms are already well known. For example $V^{vac}(r)$ is[6]

$$V^{vac}(r) = \lambda \frac{e^2}{r} \int_{4m_e^2}^{\infty} dt \, \frac{e^{-r\sqrt{t}}}{2t} (1 + \frac{2m_e^2}{t}) \sqrt{1 - \frac{4m_e^2}{t}} \tag{3}$$

, where m_e is the mass of the electron, and $\lambda = 2\alpha/3\pi = 1.549 \times 10^{-3}$. Therefore what we are going to determine is the remainder $\tilde{V}(r)$. Hereafter the tilde indicates the quantities in which the Coulomb, the vacuum polarization and the one-pion exchange contributions are separated. It is convenient to represent the potential as the superposition of the states exchanged with mass $\sqrt{t'}$:

$$\tilde{V}(r) = -\frac{1}{\pi M^2} \frac{1}{r} \int_0^{\infty} dt' \tilde{A}_t(s,t') e^{-r\sqrt{t'}} \quad with \quad s = 4M^2 \, . \tag{4}$$

, in which s is fixed at the threshold value $4M^2$ in order to avoid the weak momentum dependency of the potential[17].

In the integral representation of the scattering amplitude $\tilde{A}^{(\pm)}(s,t)$, the same spectral function $\tilde{A}_t(s,t')$ appears, namely

$$\tilde{A}^{(\pm)}(s,t) = \frac{1}{\pi} \int_0^{\infty} dt' \frac{\tilde{A}_t(s,t')}{t'-t} \pm \frac{1}{\pi} \int_0^{\infty} du' \frac{\tilde{A}_u(s,u')}{u'-u} \tag{5}$$

, where the u-channel spectral function $\tilde{A}_u$ is the same as that of the t-channel, namely $\tilde{A}_u(s,*) = \tilde{A}_t(s,*)$. The plus and minus signs between the integrations of Eq.(5) correspond to the spin singlet and the spin triplet states respectively. The coefficient appeared in front of the integration of Eq.(4) can be checked by making the Fourier transformation $\int d^3r \exp[-i\vec{K} \cdot \vec{r}] \cdots$ of Eq.(4) to obtain the first term of Eq.(5), in which the momentum transfer vector $\vec{K}$ relates to the Mandelstam variable t by

$$t = -|\vec{K}|^2 = -2\nu(1 - \cos\theta). \tag{6}$$

The second term of the r.h.s. of Eq.(5) is obtained by simply replacing t by u, where $u = -2\nu(1 + \cos\theta)$.

In Eq.(4), the lower limit of the integration is $4\mu_\pi^2$ for the case of the meson theory, whereas it is zero for the case of the long range potential, and moreover the asymptotic behavior of the potential $V(r) \sim -C/r^\alpha$ is solely determined by the threshold behavior of the spectral function $\tilde{A}_t(4M^2,t') = \pi C' t'^\gamma + \cdots$. They are related by

$$\alpha = 2\gamma + 3 \tag{7}$$

and

$$C = C' \frac{2\Gamma(2\gamma+2)}{M^2}. \tag{8}$$

For the case of the van der Waals potential of the Casimir-Polder type, the power α of the potential is 7, therefore the power γ of the threshold behavior of $\tilde{A}_t(4M^2,t')$ is 2.0 .

In Section 2, we shall search for the spectral function for small t' with the form of three free parameters:

$$\tilde{A}_t(4M^2, t') = \pi C' t'^{\gamma} e^{-\beta t'} \tag{9}$$

, by fitting to the once subtracted Kantor amplitude of the S-wave[7]. It turns out that $\gamma = 1.55 \sim 2.0$, and it is consistent with the van der Waals force. For wider range of t', the spectral function is reproduced well by a functional form with more parameters, and we shall use these parameters when we calculate the interference pattern in Section 3. They are :

$$\frac{1}{\pi}\tilde{A}_t(4M^2, t) = \begin{cases} (A_2 t^2 + A_3 t^3)e^{-\beta_a t} + B_3 t^3 e^{-\beta_b t} & in\ t < 16 \\ (\sum_{j=2}^{6} C_j t^j)e^{-\beta_c t} & in\ t > 16 \end{cases} \tag{10}$$

, where the values of parameters are

$$\beta_a = 0.346, \quad A_2 = 0.603, \quad A_3 = -2.824 \times 10^{-2}$$

$$\beta_b = 3.20 \times 10^{-4}, \quad B_3 = 1.625 \times 10^{-4}$$

$$\beta_c = 0.0124, \quad C_2 = 3.889 \times 10^{-2}, \quad C_3 = -4.517 \times 10^{-3}$$

$$C_4 = 1.638 \times 10^{-4}, \quad C_5 = -1.170 \times 10^{-6}, \quad C_6 = 1.862 \times 10^{-9}$$

, hereafter units of masses are the mass of the neutral pion, unless the use of other unit is stated explicitely.

Finally, it will be helpful to write the differential cross section $\sigma(\theta)$ of the proton-proton scattering explicitely[8].

$$\begin{aligned} &\nu\sigma(\theta) \\ &= \frac{1}{4}|f^s(\theta) + 2exp[i\delta_0^E]\sin\delta_0^E + \alpha_{even}(z)|^2 + \\ &+ \frac{3}{4}|f^t(\theta) + 6\delta_{1C}z + \alpha_{odd}(z)|^2 + \Delta \end{aligned} \tag{11}$$

, where δ_{1C} is the central P-wave phase shift, and Δ is the contribution from the noncentral amplitudes, which do not interfere with the Coulomb amplitude. α_{even} and α_{odd} come from the higher partial waves other than the OPE contributions. f^s and f^t are the spin singlet

and the spin triplet amplitudes respectively, which arise from the Coulomb and the one-pion exchange potentials. If we use variables $s = \sin(\theta/2)$, $c = \cos(\theta/2)$ and $\eta = e^2/\hbar v_L$, their explicite forms are

$$\begin{aligned} &f^s(\theta) = \\ &- \frac{\eta}{2}\{\frac{1}{s^2}\exp[-i\eta\ln s^2] + \frac{1}{c^2}\exp[-i\eta\ln c^2]\} + \\ &+ f^2 M\sqrt{\nu}\{(\frac{1}{1-t} + \frac{1}{1-u}) - \frac{2}{2\nu}Q_0(1+\frac{1}{2\nu})\} \end{aligned} \tag{12}$$

and

$$\begin{aligned} &f^t(\theta) = \\ &- \frac{\eta}{2}\{\frac{1}{s^2}\exp[-i\eta\ln s^2] - \frac{1}{c^2}\exp[-i\eta\ln c^2]\} + \\ &- \frac{f^2}{3}M\sqrt{\nu}\{(\frac{1}{1-t} - \frac{1}{1-u}) - \frac{6}{2\nu}Q_1(1+\frac{1}{2\nu})z\} \end{aligned} \tag{13}$$

,where v_L is the velocity in the labratory system. In the one-pion exchange (OPE) terms, the S and P waves are subtracted.

In summary our task is to observe the effects of the singularity at $t = 0$ in the forward region, and in particular for the case of the van der Waals force of the Casimir-Polder type, the form of the singularity is $C't^2\ln(-t)$.

2. The Kantor Amplitude Simplified

In this section, we shall consider scatterings by a short range potential, and inclusion of the Coulombic potential will be done only in the final part of this section when we tabulate the Kantor amplitude of the S-wave of the p-p scattering. It is well-known that

$$X_\ell(\nu) = \nu^{\ell+1/2}\cot\delta_\ell(\nu) \tag{14}$$

is regular at $\nu = 0$, and can be expanded in terms of ν. Partial wave amplitudes relate to the phase shifts $\delta_\ell(\nu)$ in the elastic region by

$$h_\ell(\nu) = \frac{\sqrt{M^2+\nu}}{\sqrt{\nu}}e^{i\delta_\ell(\nu)}\sin\delta_\ell(\nu). \tag{15}$$

From Eqs.(14) and (15),

$$\frac{h_\ell(\nu)}{\nu^\ell} = \frac{\sqrt{M^2+\nu}}{X_\ell(\nu) - i\sqrt{\nu}\,\nu^\ell} \tag{16}$$

Since we analyse the S-wave amplitude in this paper, we set $\ell = 0$ hereafter, however equations for the higher partial waves are recovered if $h_0(\nu)$ is replaced by $h_\ell(\nu)/\nu^\ell$. The integral representation of the partial wave amplitude is

$$h_0(\nu) = \frac{1}{\pi}\int_{-\infty}^{-a/4} \frac{Im\, h_0(\nu')}{(\nu'-\nu)}d\nu' + \frac{1}{\pi}\int_0^\infty \frac{Im\, h_0(\nu')}{(\nu'-\nu)}d\nu' \tag{17}$$

where $\sqrt{a}$ is the smallest mass of the exchanged states. The right hand cut ($\nu > 0$) is the unitarity cut and whose spectral function $Imh_0(\nu')$ is determined directly from the phase shift data. By collecting the terms, which are calculated from the experimental data, in the integral representation of Eq.(17), the Kantor amplitude $K_0(\nu)$ is introduced by[9]

$$K_0(\nu) = h_0(\nu) - \frac{1}{\pi}\int_0^\infty \frac{Im\, h_0(\nu')}{(\nu'-\nu)}d\nu' \tag{18}$$

, and Eq.(17) becomes

$$K_0(\nu) = \frac{1}{\pi}\int_{-\infty}^{-a/4} \frac{Im\, h_0(\nu')}{(\nu'-\nu)}d\nu' . \tag{19}$$

Equation(19) indicates $K_0(\nu)$ is regular at $\nu = 0$, and the nearest singularity occurs at $\nu = -a/4$. For p-p scattering, $a = \mu_0^2$, where μ_0 is the mass of the neutral pion. When we need the wider domain of analyticity, we subtract the contribution of the one-pion exchange, then a moves to $4\mu_0^2$, which corresponds to the threshold of the two-pion exchange spectrum. When we calculate $K_0(\nu)$ for real positive values of ν, we must evaluate the pricipal value integration in Eq.(18), however the direct numerical integration is extemely difficult because the "anti-bound state" causes the rapid change of $\delta_0(\nu)$, and it does not respect the ordinary threshold behavior except in the region of extremely small value of ν.

However the difficulty is bypassed, if we first calculate $K_0^{eff}(\nu)$. We introduce a polynomial $X_0^{eff}(\nu)$, which is the effective range expansion of $X_0(\nu)$ defined in Eq.(14). $h_0^{eff}(\nu)$ and $K_0^{eff}(\nu)$ are obtained from Eqs.(16) and (18) simply by substituting $X_0(\nu)$ by $X_0^{eff}(\nu)$.

We point out that from Eq.(16) $h_0^{eff}(\nu)$ is a meromorphic function* on the k-plane, where $k = \sqrt{\nu}$. The upper half k-plane corresponds to the first sheet of ν. We claim

$$K_0^{eff}(\nu) = \sum_j \frac{Res(h_0^{eff}(\nu_j))}{(\nu-\nu_j)} \tag{20}$$

, where $Res(h_0^{eff}(\nu_j))$ are the residues of the poles, and the sum extends to all the poles on the first sheet of ν. This is shown by writing the Kantor amplitude in the form of the contour integration :

$$K_0(\nu) = -\frac{1}{2\pi i}\int_C d\nu' \frac{h_0(\nu')}{\nu'-\nu} \tag{21}$$

, where the contour C is given in Figure 1. When $X_0(\nu')$ is a polynomial of ν', such as $X_0^{eff}(\nu')$, then the singularities in the closed contour C are the poles of $h_0(\nu')$. Therefore we can evaluate the contour integration by using the positions of the poles and their residues. The numerical evaluation of the correction to $K_0^{eff}(\nu)$ to obtain $K_0(\nu)$ is straightforward, because the spectral function of the principal value integration is $Im(h_0(\nu') - h_0^{eff}(\nu'))$, which does not involve the dominant effect of the "anti-bound state".

Finally, in order to guarantee the convergence of the integral representation Eq.(17) of the S-wave amplilude, we shall consider the once subtracted form of the Kantor amplitude $K_0^{(1)}(\nu)$, which is

$$K_0^{(1)}(\nu) \equiv \frac{K_0(\nu) - K_0(0)}{\nu}. \tag{22}$$

From the effective range parameters and the phase shift data, we can determine the precise values of the once subtracted Kantor amplitude $K_0^{(1)}(\nu)$ by

$$K_0^{(1)}(\nu) = \sum_j \frac{Res(h_0^{eff}(\nu_j))}{\nu_j(\nu-\nu_j)} + [\Delta K_0^{(1)}(\nu)]_R + [\Delta K_0^{(1)}(\nu)]_I \tag{23}$$

, where the corrections consist of two terms, which come from the real and imaginary part of $(h_0(\nu) - h_0^{eff}(\nu))$ respectively. They are

*Strictly speaking, this is true in the nonrelativistic approximation in which $\sqrt{m^2+\nu}$ in Eq.(16) is replaced by m.

$$[\Delta K_0^{(1)}(\nu)]_R = Re(\frac{h_0(\nu) - h_0(0)}{\nu} - \frac{h_0^{eff}(\nu) - h_0^{eff}(0)}{\nu}) \tag{24}$$

, and

$$[\Delta K_0^{(1)}(\nu)]_I = \frac{P}{\pi}\int_0^\infty \frac{Im(h_0(\nu') - h_0^{eff}(\nu'))}{\nu'(\nu' - \nu)} d\nu' \tag{25}$$

, where P stands for the principal value integration.

Inclusion of the Coulombic force is not difficult and is publised in a separate paper[7]. Using the phase shift data of the Nijmegen group[10][11] supplemented by the data of Arndt et. al.[12][13][14] in the higher energy region, the Kantor amplitude was calculated and tabulated. In Table 1, the once subtracted S-wave Kantor amplitude $K_0^{(1)}(\nu)$ is given, in which the one-pion exchange contribution is subtracted. We can use the Table of the Kantor amplitude, as in the same sense as the phase shift $\delta_0^E(\nu)$ or the effective range function $X_0(\nu)$ introduced in Eq.(14). However $K_0^{(1)}(\nu)$ is more suitable to investigate the property of the potential acting between protons, because the spectral function $\tilde{A}_t(4M^2, t')$ is related to the Kantor amplitude by

$$\tilde{K}_0^{(1)}(\nu) = \int_0^\infty dt' \tilde{A}_t(4m^2, t')\frac{1}{\nu}[\frac{1}{4\nu}\log(1 + \frac{4\nu}{t'}) - \frac{1}{t'}]. \tag{26}$$

, where the tilde indicates the subtraction of the one-pion exchange term. Equation (4) indicates the potential is the Laplace transformation of the spectral function appeared in Eq.(26). Therefore the Kantor amplitude and the nuclear potential are related linearly by the mediation of the spectral function $\tilde{A}_t(4m^2, t')$. This is the merit to use the Kantor amplitude rather than the phase shift or the effective range function $X_0(\nu)$, because the phase shift is disturbed by the "anti-bound state". Concerning the effective range function we can not separate the one-pion exchange term from $X_0(\nu)$ without knowing the finite back ground term of the pion pole. We emphasize that the separation of the OPE term is important to expose the effect of the long range force, and to make it easy to obseve it.

Figure 2 and 3 are the curves of $\tilde{K}_0^{(1)}(\nu)$, in which we can see an huge cusp of the attractive sign at $\nu = 0$, which can not be attributed to the short range force of the two-pion exchange. Using Eq.(26), we searched the spectral function from the data of

the Kantor amplitude, the results are given in Eq.(10). In figure 4, the spectral function $\tilde{A}_t(4M^2, t)$ devided by t is shown. Figure 5 is the graph of the once subtracted amplitude of $\tilde{A}(s,t)$, namely of

$$\frac{\tilde{A}(s,t) - \tilde{A}(s,0)}{t} = \frac{1}{\pi}\int_0^\infty dt' \frac{\tilde{A}_t(s,t')}{t'(t'-t)} \tag{27}$$

,where s is fixed at $4M^2$.

3. Angular Distribution of the Low Energy p-p Scattering

Since we have determined the spectral function $\tilde{A}_t(4M^2, t')$, which is given in Eq.(10), we can evaluate the angular distribution of the low energy proton-proton scattering. In order to observe the destructive interference pattern[15] arising from the long range force of the attractive sign and the repulsive Coulomb force, we must first construct the cross section $\sigma^{extrap}(\nu, \theta)$, which is expected to occur if the nuclear force is the short range nature and the amplitude does not posess the singularity at $t = 0$. In the meson theory of the nuclear force, the nearest singularity of the amplitude $\tilde{A}(s,t)$ occurs at $t = 4$, which corresponds to the threshold of the two-pion exchange. Therefore on the compex z-plane the amplutudes $\tilde{A}(s,t)$ are regular in

$$-(1 + 2/\nu) < z < (1 + 2/\nu). \tag{28}$$

and for the low energy scattering ($\nu < 1$), we have wide domain of analyticity, and the amplitude in the physical region $-1 \leq z \leq 1$ can be reproduced well by a few terms of a polynonial of z.

On the other hand, if the long range force is involved, the amplitudes have singularities at $t = 0$ and at $u = 0$, namely in terms of the z variable the singularities occur at $z = \pm 1$. To confirm the long range force is to observe the singularities, whose locations are at the end points of the physical region, by comparing the amplitude with what is expected in the case of the short range force. For such a purpose, after we obtain the precise data

of the cross section of the angular distribution, what we have to do are the followings. Firstly, we divide the data into two groups, the forward group ($\theta \leq \theta_{min}$) and the middle angle group ($\theta_{min} < \theta \leq 90°$). Secondly by using the formulae of the cross section of Eq.(11), we make the exprapolation of the cross section from the middle angular region to the forward region. When we use Eq.(11), α_{even} and α_{odd} are the polynomials of z of the even power and the odd power respectively, and whose coefficients are fixed by fitting to the data in the middle angular region. Thirdly we take the difference of the measured cross section and the extrapolated cross section in the forward region:

$$\Delta\sigma(\nu,\theta) = \sigma(\nu,\theta) - \sigma^{extrap}(\nu,\theta). \tag{29}$$

When the destructive interference exits a negative cusp in $\Delta\sigma(\nu,\theta)$ must appear at $\theta = 0$. If we consider the ratio $R(\nu,\theta)$

$$R(\nu,\theta) = \Delta\sigma(\nu,\theta)/\sigma(\nu,\theta) \tag{30}$$

, the cusp changes to a dip in the forward region, because of the Coulombic terms in $\sigma(\nu,\theta)$. In order to find the most suitable energy region and the required precision of the measurements, the ratio R are calculated for various incident energies T_{lab}. In the calculation the ampltides $\tilde{A}^{(+)}$ and $\tilde{A}^{(-)}$ of Eq.(5) are evaluated by using the spectral function of Eq.(10) determined from the Kantor amplitude, and then the cross section is determined from Eq.(11) in which α's are chosen to be

$$\alpha_{even} = \tilde{A}^{(+)} - (polynomial\ \ of\ \ z^2)$$

and

$$\alpha_{odd} = \tilde{A}^{(-)} - z(polynomial\ \ of\ \ z^2)$$

, where the polynomials are to be subtracted to minimize the deviatin of $\Delta\sigma$ from zero in the middle angular region. The patterns of R turn out to be common, namely in the middle region of the angle $\theta_{min} < \theta < 180° - \theta_{min}$, R is close to zero, as it must be,

and on the other hand R has a dip in the forward region whose minimum occurs around $\theta = 12°$. The depth of the dip depends on the energy T_{lab}.

The favorable energy range to measure is relatively narrow:

$$25MeV. \leq T_{lab} \leq 30MeV. \tag{31}$$

To understand the situation, four figures (fig.6 $\sim$ fig.9) of $\Delta\sigma(\nu,\theta)/\sigma(\nu,\theta)$ are shown for fiexd energies of 20, 25, 30 and 40 MeV. respectively, in which minimum angle of the middle angular region is chosen to be $\theta_{min} = 30°$. The depths of the dips are -0.15%, -0.26%, -0.42% and -0.29% respectively. Since the strength of the singularity at $z = 1$ is proportional to ν^2 for the case of the van der Waals force of the Casimir-Polder type, as the incident energy decreases it becomes more and more difficult to observe the dip of the destructive interference. However the higher incident energy does not necessarily mean the easiness of the observation of the dip, as we can see the situation in the figure of $T_{lab} = 40MeV.$. It is true that for fixed L_{max}, the highest power of the polynomial fitted to the amplitude $\tilde{A}(s,t)$ in the middle angular region, the depth of the dip increases with the energy. However the error in the middle angular region also increases and exceeds the allowed limit, and therefore we must increases L_{max} by one, namely in this case L_{max} must be changed from 4 to 5. Then as the figure of $T_{lab} = 40MeV.$ indicates, the depth changes from -0.82% to -0.29%. Therefore there is no merit to increase the incident energy T_{lab}, moreover in general as the energy increases the uncertainty in the estimations of the non-central amplitudes also increases. From these reasons, the recommended energy is ristricted to somewhere around $T_{lab} = 25 \sim 30MeV.$.

The figure of $T_{lab} = 25MeV.$ indicates that the requirement of the precisins are 0.05% in $30° < \theta \leq 90°$ and 0.06% in the forward region of $\theta < 30°$, because the depths and the locations of the bottoms are -0.27% and $12°$ for $L_{max} = 3$, and -0.26% and $14°$ for $L_{max} = 4$ respectively. And in order to see the bottom, measurement of the small angular region down to $\theta = 10°$ is essential. In the same way, for $T_{lab} = 30MeV.$ the required precisions are 0.05% in $30° < \theta \leq 90°$ and 0.10% in the forward region of $\theta < 30°$, because

the depths and the locations of the bottoms are -0.42% and $12°$ for $L_{max} = 3$, and -0.42% and $13°$ for $L_{max} = 4$ respectively. In this energy, measurements of the cross section in the smaller angular region is also required.

In this way, we found that in order to confirm the destructive interference pattern of the attractive long range force of the nuclear interaction and the repulsive Coulombic force, two rather challenging requirements must be fulfilled, namely one is the precision (0.05%), and the other is the measurement of the forward region (down to 10° of the scattering angle of the center of the mass system). However there is one thing to make the experiments easier, since we are going to measure the shape of the interference pattern, the high precision of the normalization of the incident beam is not necessarily required.

4. Conclusions and Comments

In the hadron physics, the low energy proton-proton scattering occupy a special position because of its high precision of the measurement, in fact in some of the measurements of the cross section of the p-p scattering[21][22], the accuracy exceeds 0.1%. I think we are now approaching to the point where we can confront the high precision data with the fundamental assumptions of the hadron physics, such as the structure of the spectrum.

By using the phase shift data, the once subtracted S-wave Kantor amplitude $\tilde{K}_0^{(1)}(\nu)$ is calculated (see Table 1 and figures 4 $\sim$ 5). $\tilde{K}_0^{(1)}(\nu)$ has the characteristic cusp at $\nu = 0$ of the long range force of the attractive sign. Various types of searches of the spectral function $\tilde{A}_t$ to fit to the Kantor amplitude have been carried out. It turns out that the power γ of the threshold behavior is $1.55 \sim 2.0$. In terms of the asymptotic behavior of the potential $V(r) \sim -C/r^\alpha$ there remains only two possibilities $\alpha = 6$ and $\alpha = 7$, if the power α is to be an integer, they corresponds to the van der Waals potential of the London type and the Casimir-Polder type respectively. If we consider the universal nature of the van der Waals interaction, we can expect that the forces of the same type must appear in other reactions such as π-N and π-π. However since the accuracy of the measurements

of such reactions are not very high, we must subtract the two-pion exhange spectrum in order to observe the effects of the long range forces.[18][19][20]

The type of the singularity in the amplitude $\tilde{A}(s,t)$ at $t = 0$ is specified by the threshold dehavior of the spectral function. For the case of $\gamma = 2$, the leading singularity is $C't^2 \ln(-t)$. If we substitue $t = -2\nu(1-z)$ into the amplitude, the leading singularity becomes

$$A(s,t) = 4C'\nu^2(1-z)^2\ln(2\nu) + 4C'\nu^2(1-z)^2\ln(1-z) + \cdots. \tag{32}$$

The first term of the r.h.s. becomes the singularity of the type $\nu^2 \ln \nu$ in the partial wave ampitudes, whereas the second term is the singularity at $z = 1$. In this paper, we proposed to observe the latter singularity as the inerference pattern with the Coulombic term. The importance of measuring the angular distribution in search of such an interference is that it can be done by a single experiment, whereas the phase shift function and the Kantor amplitude are obtained by the analysis of several different experiments.

At this point I must emphasize that the long range force observed in the Kantor amplitude is not a small correction to the short range force in the nuclear force. This is because the total value of the once subtracted Kantor amplitude of the S-wave at $\nu = 0$ is -12.02, while the contribution[16] from the one-pion exchange is -7.20 , and the remainder -4.82 is attributed to the long range force.

Finally, when the strong van der Waals force appears in the hadron-hadron interaction, and the van der Waals force arises as the secondary force of the basic Coulomb interaction between the constituent particles, it is tempting to regard the 'charge' of the basic Coulombic force as the colour. However after the strength C of the van der Waals potetial is known, there is a lower bound of the coupling constant $^*e^2$ of the basic Coulomb force, which is around 10. Therefore the coupling constant of the QCD seems to be too small. On the other hand Dirac's magnetic monopole, whose coupling constant is $^*e^2 = 137/4$, will be a good candidate[2]. Therefore the confirmation of the long range force in the nuclear force may cause a drastic change of the hadron physics.

Figure Captions

Fig.1 The contour C of the integration on ν' in Eq.(21).

Fig.2 $-\{K_0^{(1)}(\nu) - K_0^{(1),1\pi}(\nu)\}$ is plotted against T_{lab}. The curve is the column [.c30] of Table 1. The dash curve is the one-pole fit to the data in $50Mev. < T_{lab} < 240Mev.$ with an additional back ground constant.

Fig.3 Amplified graphs of the low energy region in the box of fig.2. are displayed. The curve is [.c30] of Table 1, whereas the the open circles and the closed circles are the column [.c25] and [.c35] of the Table 1, respectively. The dash curve is the same as that of fig.2. The cusp at $\nu = 0$ indicates the long range force with attractive sign.

Fig.4 The spectral function $\tilde{A}_t(4M^2, t)$ devided by t is plotted against t.

Fig.5 The once subtracted amplitude $(\tilde{A}(s,t) - \tilde{A}(s,0))/t$ is plotted against $-t$, where s is fixed at $4M^2$.

Fig.6 The interference patterns $\Delta\sigma/\sigma$ are plotted against θ_{cm}. The incident energy is $T_{lab} = 20MeV.$. L_{max} is the power of the polynomial of z fitted in the middle angular region of $30° \leq \theta \leq 150°$.

Fig.7 The same graph as fig.6 for $T_{lab} = 25MeV.$.

Fig.8 The same graph as fig.6 for $T_{lab} = 30MeV.$.

Fig.9 The same graph as fig.6 for $T_{lab} = 40MeV.$.

Table Caption

Table 1 The first column is the incident energy T_{lab} in Mev.. The second column is $X_0(\nu)$. The third, fourth and fifth columns are $\{K_0^{(1)}(\nu) - K_0^{(1),1\pi}(\nu)\}$, in which the adopted effective range parameters are obtained by fitting to the data in $0.25 \leq T_{lab} \leq 3.0$, $0.30 \leq T_{lab} \leq 3.0$ and $0.35 \leq T_{lab} \leq 3.0$ in Mev. respectively. The sixth column is the

error of $h_0(\nu)/\nu$, and which is useful to estimate the error of the once subtracted Kantor amplitude, namely $\Delta K_0^{(1)}(\nu)$.

References

[1] H. Yukawa , Proc. Phys. Math. Soc. Japan **17** , 98 , (1935)

[2] J. Schwinger , Science **165** ,757 , (1969)
A. O. Barut , Phys. Rev. **D3** , 1747 , (1971)
T. Sawada , Phys. Lett. **B43** , 517 ,(1973)

[3] P. A. M. Dirac , Proc. R. Soc. London **A133** , 60 , (1931)

[4] T. Sawada , Phys. Lett. **43B** , 517 , (1973)

[5] T. Sawada , Nucl. Phys. **B71** , 82 , (1974)
T. Sawada , Prog. Theor. Phys. **59** , 149 , (1978)

[6] L. Heller , Phys. Rev. **120** , 627 , (1960)

[7] T. Sawada , "Long Range Component of the Nuclear Force " , submitted to Phys. Rev. C , (1995)

[8] M. S. Sher, P. Signell and L. Heller , Ann. Phys. **58** , 1 , (1970)

[9] P. B. Kantor , Phys. Rev. Lett. **12** , 52 , (1964)

[10] J.R. Bergervoet, P.C. van Campen, W.A. van der Sanden and J.J. de Swart , Phys. Rev. **C38** , 15 , (1988)

[11] V.G.J. Stoks , R.A.M. Klomp , M.C.M. Rentmeester and J.J. de Swart , Phys. Rev. **C48** , 792 , (1993)

[12] R. A. Arndt, L. D. Roper, R. A. Bryan, R. B. Clark, B. J. DerWest and P. Signell , Phys. Rev. **D28** , 97 , (1983)

[13] R. A. Arndt, J. S. Hyslop III and L. D. Roper, Phys. Rev. **D35** , 128 , (1987)

[14] R. A. Arndt, L. D. Roper, R. L. Workman and M. W. McNaughton , Phys. Rev. **D45** , 3995 , (1992)

[15] T. Sawada and D. Kiang, Nuovo Cimento **77A** , 308 , (1983)

[16] O. Dumbrajs, R. Koch, H. Pilkuhn, G. C. Oades, H. Behrens, J. J. DeSwart and P. Kroll , Nucl. Phys. **B216** , 277 , (1983)

[17] G. Feinberg and J.Sucher , Phys. Rev. **139B** , 1619 , (1965)
G. Feinberg and J. Sucher , Phys. Rev. **A2** , 2395 , (1970)
J. Sucher , Cargése Lecture in Physics vol.6 , ed. M. Lévy , Gordon and Breach (1977)

[18] T. Sawada , Phys. Lett. **B100** , 50 , (1981)

[19] T. Sawada , Nuovo Cimento **62A** , 207 , (1981)

[20] T. Sawada , Prog. Theor. Phys. **63** , 2016 , (1980)
T. Sawada , Phys. Lett. **B225** , 291 , (1989)

[21] Ch. Thomann, J. E. Benn and S. Münch Nucl. Phys. **A303** , 457 , (1978)

[22] von H. Wassmer and M ühry , Helv. Phys. Acta **46** , 626 , (1973)

Table 1.

$T_{lab}(Mev.)$	$X_0(\nu)$	$K_0^{(1)}(\nu) - K_0^{(1),1\pi}(\nu)$			$\Delta h_0(\nu)/\nu$
		[.c25]	[.c30]	[.c35]	
0	.18716	-4.8701	-4.8238	-4.8172	$\cdots$
1	.21158	-4.6629	-4.6344	-4.6303	$.102 + i.223$
2	.23610	-4.4856	-4.4693	-4.4670	$.061 + i.168$
3	.25950	-4.3394	-4.3293	-4.3279	$.027 + i.121$
4	.28315	-4.2302	-4.2226	-4.2215	$.001 + i.083$
5	.30665	-4.1402	-4.1343	-4.1335	$-.019 + i.053$
6	.33008	-4.0502	-4.0453	-4.0446	$-.028 + i.034$
7	.35344	-3.9752	-3.9710	-3.9704	$-.028 + i.026$
8	.37677	-3.9084	-3.9047	-3.9042	$-.022 + i.026$
9	.40008	-3.8447	-3.8414	-3.8410	$-.014 + i.027$
10	.42344	-3.7858	-3.7829	-3.7825	$-.010 + i.026$
12	.47017	-3.6810	-3.6785	-3.6782	$-.007 + i.018$
14	.51702	-3.5886	-3.5865	-3.5863	$-.005 + i.014$
16	.56406	-3.5053	-3.5034	-3.5032	$-.004 + i.012$
18	.61135	-3.4292	-3.4275	-3.4273	$-.003 + i.011$
20	.65899	-3.3589	-3.3574	-3.3572	$-.003 + i.011$
22	.70704	-3.2933	-3.2918	-3.2916	$-.002 + i.011$
24	.75559	-3.2305	-3.2291	-3.2289	$-.002 + i.011$
26	.80471	-3.1707	-3.1694	-3.1692	$-.001 + i.009$
28	.85449	-3.1126	-3.1113	-3.1111	$-.000 + i.008$
30	.90502	-3.0508	-3.0496	-3.0495	$.0001 + i.0073$
40	1.1766	-2.8235	-2.8224	-2.8223	$.0008 + i.0052$
50	1.4735	-2.6650	-2.6642	-2.6641	$.0009 + i.0043$
60	1.7949	-2.5299	-2.5293	-2.5292	$.0014 + i.0030$
70	2.1749	-2.4075	-2.4070	-2.4069	$.0016 + i.0024$
80	2.5366	-2.2962	-2.2958	-2.2957	$.0016 + i.0022$
90	2.9706	-2.1948	-2.1944	-2.1943	$.0016 + i.0021$
100	3.459	-2.1019	-2.1015	-2.1015	$.0016 + i.0019$
120	4.662	-1.9396	-1.9393	-1.9392	$.0018 + i.0015$
140	6.296	-1.8009	-1.8006	-1.8006	$.0019 + i.0012$
160	8.66	-1.6803	-1.6801	-1.6800	$.0020 + i.0010$
180	12.4	-1.5742	-1.5740	-1.5739	$.0019 + i.0007$
200	19.3	-1.4797	-1.4796	-1.4795	$.0018 + i.0004$
220	36.1	-1.3951	-1.3949	-1.3949	$.0016 + i.0002$
240	142.	-1.3185	-1.3184	-1.3184	$.0015 + i.0001$

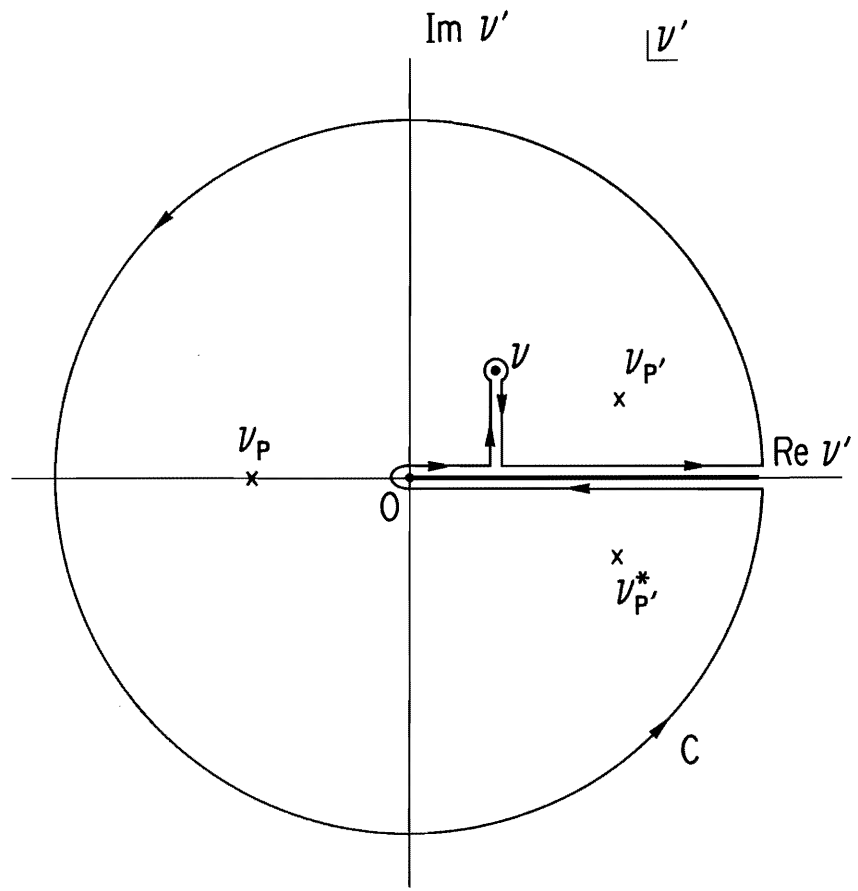

Fig 1

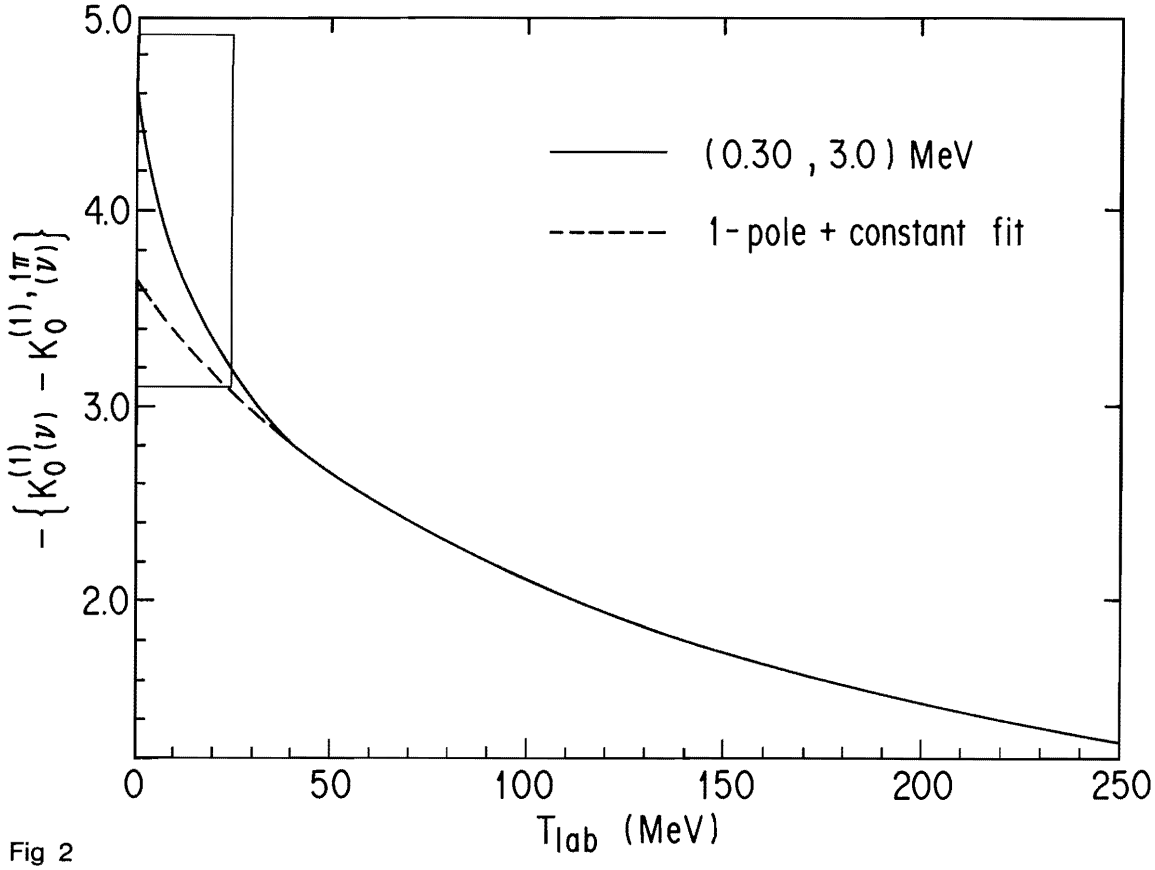
5.0
4.0
3.0
2.0
0
50
100
150
200
250
T_{lab} (MeV)
$-\{K_0^{(1)}(\nu) - K_0^{(1),1\pi}(\nu)\}$
(0.30 , 3.0) MeV
1-pole + constant fit

Fig 2

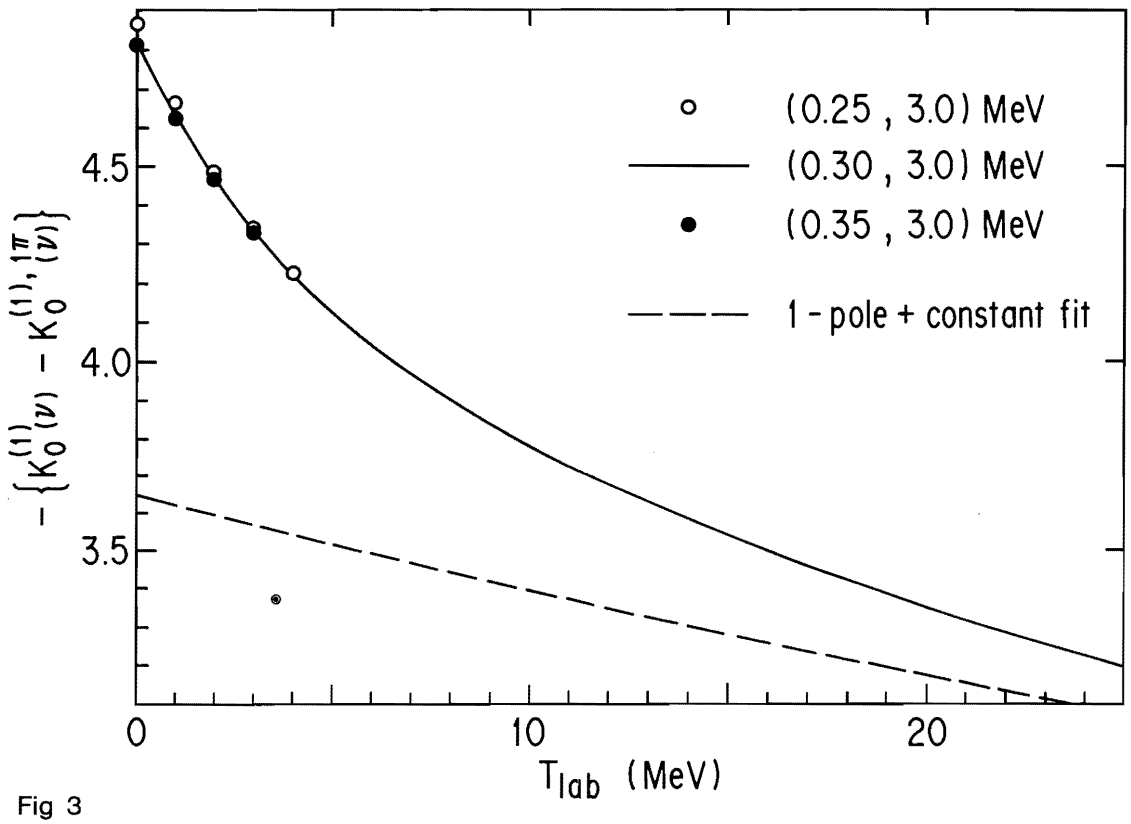
4.5
4.0
3.5
0
10
20
T_{lab} (MeV)
$-\{K_0^{(1)}(\nu) - K_0^{(1),1\pi}(\nu)\}$
(0.25 , 3.0) MeV
(0.30 , 3.0) MeV
(0.35 , 3.0) MeV
1-pole + constant fit

Fig 3

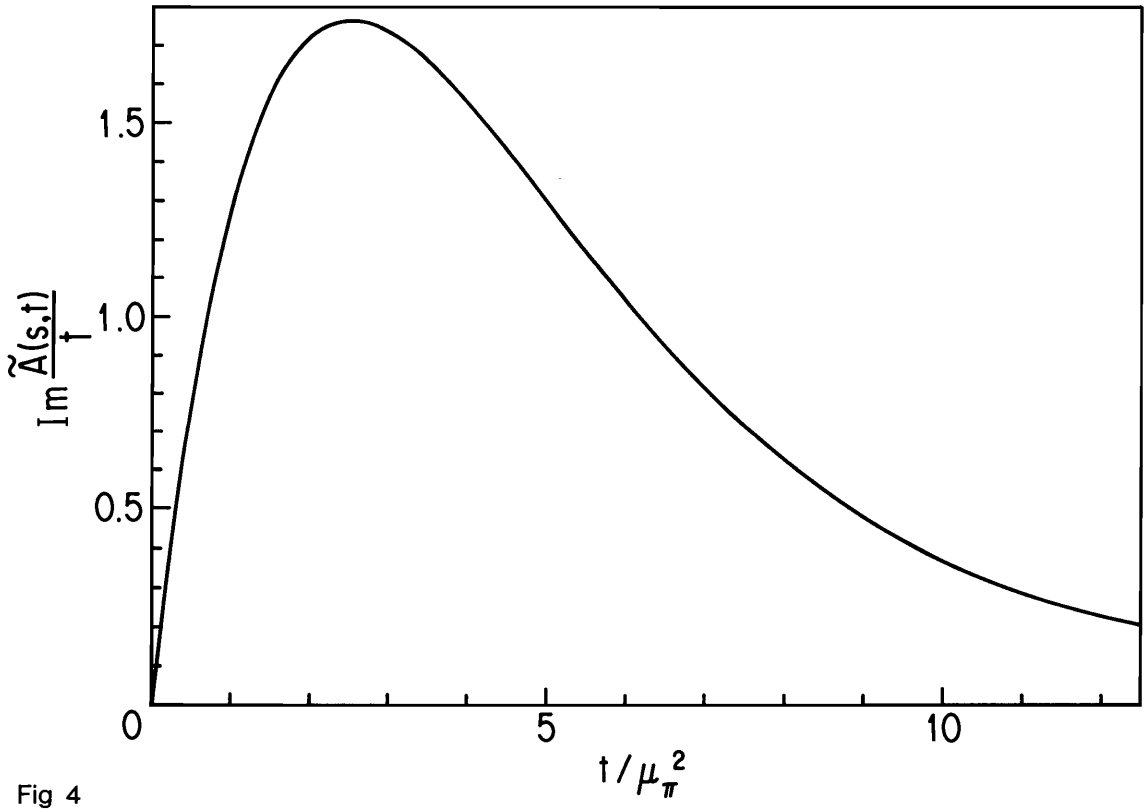
1.5
1.0
0.5
0
5
10
$\mathrm{Im}\,\frac{\tilde{A}(s,t)}{t}$
t/μ_π^2

Fig 4

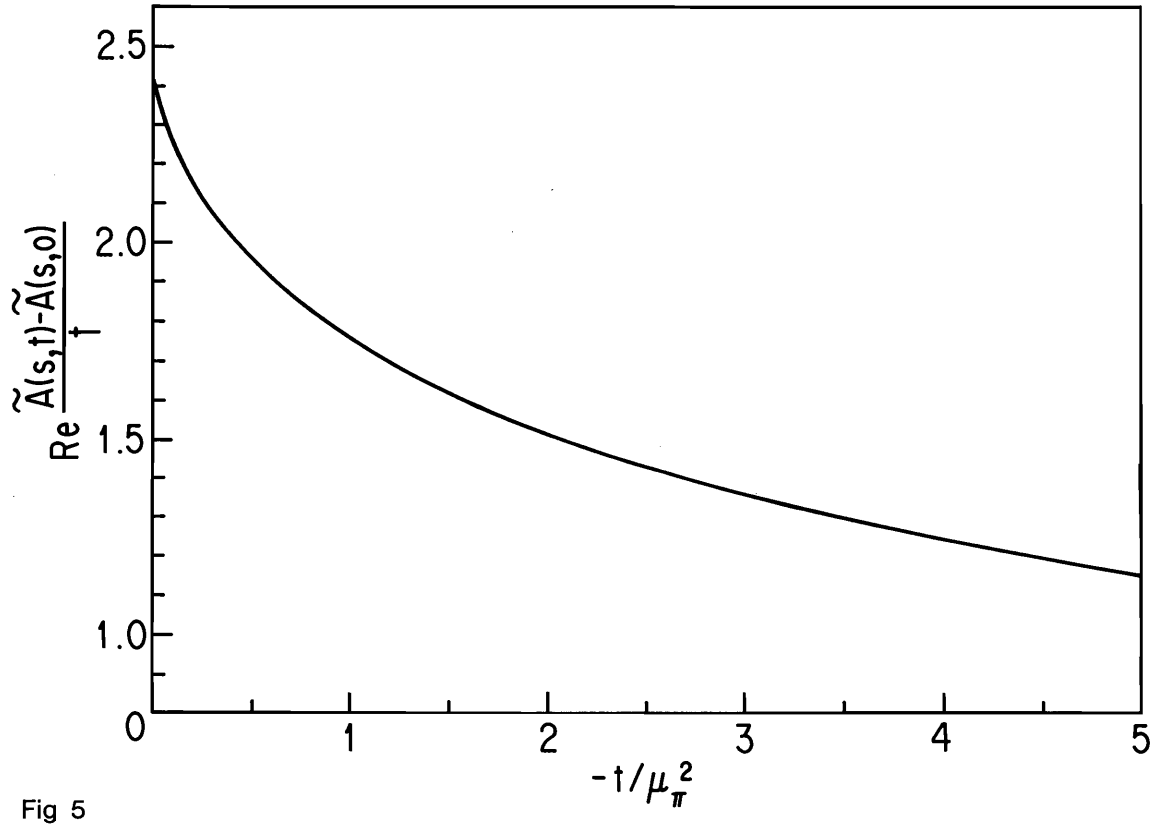
2.5
2.0
1.5
1.0
0
1
2
3
4
5
$\mathrm{Re}\,\frac{\tilde{A}(s,t)-\tilde{A}(s,o)}{t}$
$-t/\mu_\pi^2$

Fig 5

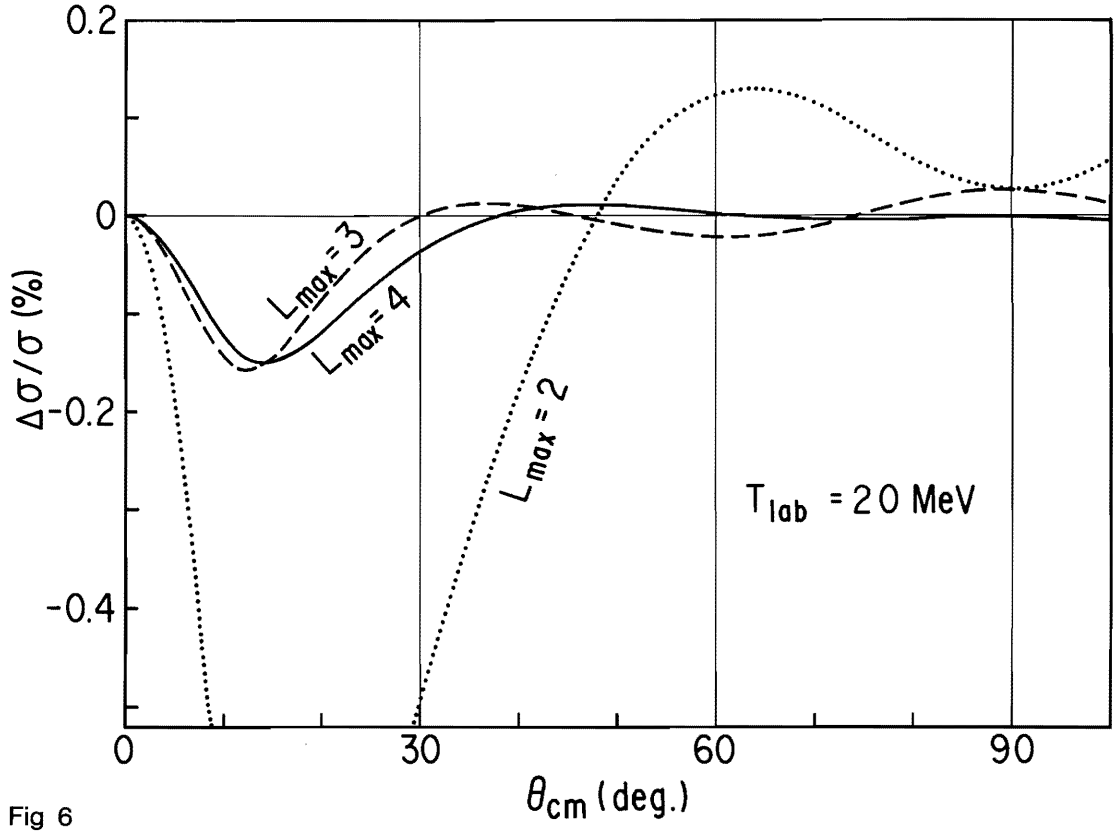
0.2
0
-0.2
-0.4
Δσ/σ (%)
0
30
60
90
θcm (deg.)
Lmax = 3
Lmax = 4
Lmax = 2
Tlab = 20 MeV

Fig 6

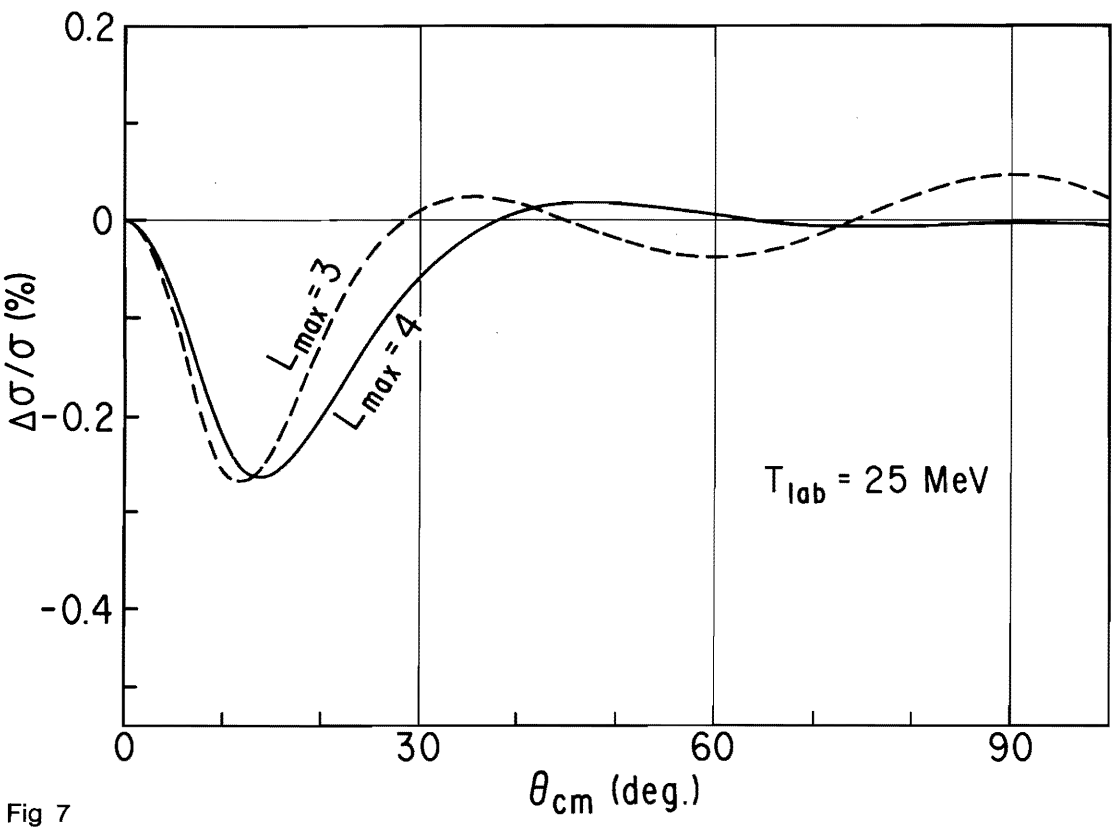
0.2
0
-0.2
-0.4
Δσ/σ (%)
0
30
60
90
θcm (deg.)
Lmax = 3
Lmax = 4
Tlab = 25 MeV

Fig 7

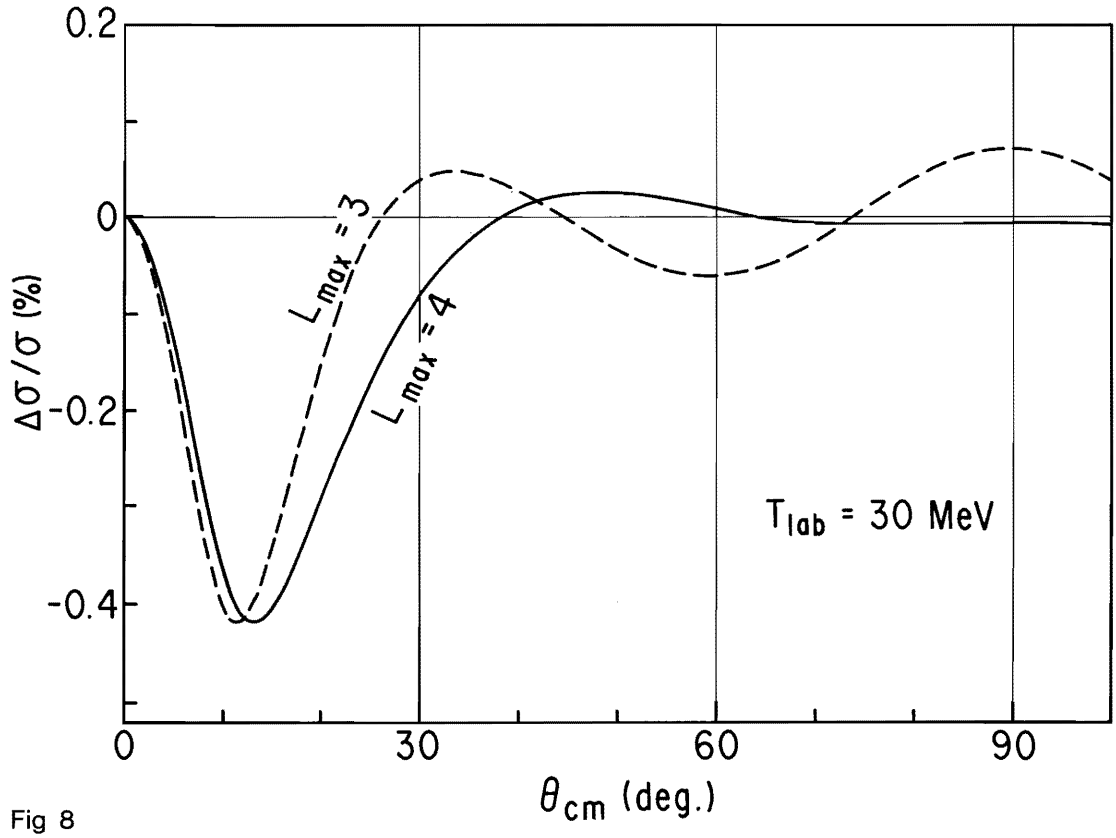
0.2
0
-0.2
-0.4
Δσ/σ (%)
0
30
60
90
θcm (deg.)
Lmax = 3
Lmax = 4
Tlab = 30 MeV

Fig 8

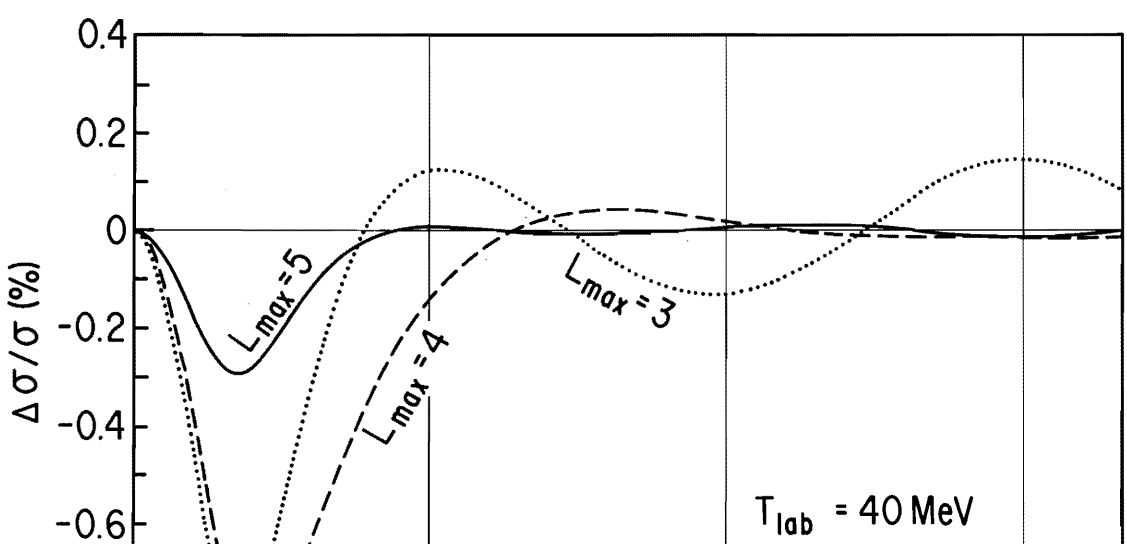
0.4
0.2
0
-0.2
-0.4
-0.6
Δσ/σ (%)
Lmax = 5
Lmax = 4
Lmax = 3
Tlab = 40 MeV